

## Pressure Pulsation Characteristics of Tidal Turbine Using Bidirectional Fluid-Solid Coupling

Mengshang Zhao<sup>1</sup>, Nina Wang<sup>2</sup>, Decheng Wan<sup>3\*</sup>

<sup>1</sup> School of Ocean Engineering and Technology, Sun Yat-Sen University, Zhuhai, Guangdong, China

<sup>2</sup> Key Laboratory of Far-shore Wind Power Technology of Zhejiang Province,  
Power China Huadong Engineering Corporation Limited, Hangzhou, China

<sup>3</sup> Computational Marine Hydrodynamic Lab (CMHL), School of Naval Architecture, Ocean and Civil Engineering,  
Shanghai Jiao Tong University, Shanghai, China

\*Corresponding author

### ABSTRACT

The purpose of this research is to study the pressure pulsation and structural characteristics of the tidal turbine based on bidirectional fluid-solid coupling at three different rotational speeds. The results indicate that the pressure pulsation increases as the increase of rotational speeds, the main frequency of pressure pulsation coefficient is blade frequency, the pressure pulsation at the downstream blade is much stronger. Blade tip develops a maximum deformation and maximum equivalent stress is located near the blade root. Prestress has little influence on the modal orders of tidal turbines. The turbine's modal deformation, from first to third is dominated by a single blade's flapping motion, from fifth to sixth is a couple of flapping and sway.

**KEY WORDS:** tidal turbine; pressure pulsation; bidirectional fluid-solid coupling; blade deformation; modal analysis.

### INTRODUCTION

The problems of environmental pollution and the demand for energy attract people's attention dramatically as the social development for all countries in the world (Wang, Sun, Xu, Liu and Bai, 2017). It provides a new way to reduce environmental pollution for us to use clean renewable energy as energy supply under the background of massive energy consumption. In recent years, with the rapid development of renewable energy such as solar energy, wind energy, marine energy and so on, marine energy has attracted worldwide attention because of its rich reserves and much lower level of development. Tidal current energy, as a kind of marine energy, has attracted many scholars' attention for its unique advantages such as high energy density, accurate predictability and no unrestricted by seasons. Horizontal axis or vertical axis tidal current turbines are two different tidal turbines that are most widely used in the development of tidal current energy. Furthermore, horizontal axis tidal current energy is much more popular and have been adopted among most of the existing commercial tidal current power stations because of its high efficiency and stability of the torque.

The hydrodynamic characteristics are primarily concerned for the tidal turbine as the main hydraulic machinery. Tian, Ni and Zhang (2020) studied the surface wave effect on the tidal turbine through the three-dimensional transient computational fluid dynamics, the results

demonstrated the average torque increased as the growth the wave high, Zang, Zheng, Zhang, Zhang and Fernandez-Rodriguez(2019), Zhang, Zang, Zheng, Cappiotti, Zhang, Zheng and Fernandez-Rodriguez (2021) carried out model experiments to compare the different anisotropy and eddy current number at the different wave parameters, the results found wave affected the anisotropy by strengthening wake's turbulence intensity, while wave only significantly affected the eddy current number at the near wake and had little effect on it at far wake, many scholars also have done a lot of researches on the erosion of turbine with single pile at the different wave parameters. Besides, wake characteristics at different cases included the wall roughness, turbulence intensity, blocking ratio, array layout of the multi-unit array, and so on have also been discussed through model experiments and numerical simulations.

Due to the influence of waves, the floating tidal turbine may generate forced motion at different degrees of freedom, many recent studies have focused on the effect of different freedoms on the tidal turbine. Hydrodynamic characteristics of the turbine with surging and yawing coupled motions, surge motions were simulated adopted dynamic mesh technique using CFX and the formula of hydrodynamic load coefficient was obtained based on the least square method under different freedoms by (Wang, Xu, Zhu and Wang, 2014, Wang, Cui, Ye, Chen and Zhang , 2019). It was found the hydrodynamic load coefficient at coupled motion was mainly affected by the surge, the frequency of surge performed a much stronger effect on the turbine. Although both wind turbines and tidal turbines work at two different fluids (air and water), they follow the Betz' Law, so research methods on tidal turbines can often refer to the wind turbine's(Huang, Wan and Hu, 2021).

The fluid-structure coupling characteristics of tidal turbines were also studied by many researchers. Experiments and numerical simulations were also contributed to research blade deformation at yawed inflow conditions (Park, Park, and Rhee, 2016), the results demonstrated that a much larger deformation was caused near the blade tip, but the vorticity near the blade tip decreased distinctly, Ullah, Hussain, Abbas, Ahmad, Amer and Noman (2019) studied the structural characteristics for a three-blade tidal turbine based on fluid-structure coupling technology using CFX, the results indicated that the natural frequency of the turbine was far greater than external frequency under normal load, so resonance would not occur, fatigue analysis indicated that the turbine can maintain endurance under a higher load than the normal operating load, so it is

recommended to make hollow blades to reduce weight. Yang, Xiang, Fang and Pain (2019) analyzed the hydrodynamics and structural elastic response adopted adaptive grid technology based on URAN  $k\sim\epsilon$  fluid-structure coupling model, the results suggested that the model can be used to predict the flow-induced vibration and power output precisely. Khalid, Zhang, Zhang and Sun (2013) proposed a new method using APDL to improve the computational efficiency of fluid-solid coupling, besides, many studies included characteristics of fluid-solid coupling have also been done. Above all, those researches played an important role in exploiting the hydrodynamic characteristics and structural characteristics, however, the pressure pulsation characteristics of the tidal turbine based on bidirectional fluid-solid coupling was still considered unclear, those researches still need to be done.

So, this paper is concentrated on studying the pressure pulsation and structural characteristics based on the method of bidirectional fluid-solid coupling. This paper takes a three-blade tidal turbine designed by Hohai University as the research object, the flow field data was calculated using Fluent and the turbine's rotational motion was simulated through the sliding mesh. The structural field data was calculated in the Transient Structural module, the data exchange between fluid and solid through the System Coupling module, mesh of the fluid field would be deformed as the deformation of the solid blades by dynamic grid technology. The three different modules are combined in the workbench platform, also the modal module is used for modal analysis.

To fully reveal the fluid-structure coupling characteristics, the tidal turbine at different three rotational speeds were simulated, the change regulation and dominant frequency of pressure pulsation were obtained, meantime, the structural characteristics included blade deformation, equivalent stress and modal were calculated. The results are expected to enhance the knowledge of tidal turbines.

## NUMERICAL METHODS

### Simulation Model and Grid Divisi



(a) Experimental model (b) Numerical model  
Fig.1 Experimental model and numerical model

The simulation model was a three-blade tidal turbine designed by Hohai University (Zhang, Zang, Zheng, Cappiotti, Zhang, Zheng and Fernandez-Rodriguez 2021), the blades included NREL S822/S823 profiles were optimized. The variation of chord length and twist angle along the radial are shown as Table 1. Main characteristics parameters of the tidal turbine are as follow: the turbine model has a rotor with a diameter of  $D = 0.3\text{ m}$ , a cylindrical nacelle with a diameter of 50mm, the length of the nacelle of 60mm, the tidal turbine was made of 6061 aluminum, specific material property parameters are shown as Table 2. Fig. 1 was the experimental tidal turbine model and the numerical model. This tidal turbine had designed rotational speed of  $10.4\text{ rad/s}$  at a flow velocity of  $0.4\text{ m/s}$  and Reynolds number is nearly  $10^5$ .

Table 1 Radial variation of chord length and twist.  $R = D / 2$

r/R	r(mm)	c/R	$\theta(^{\circ})$	t/c(%)
0.167	30	0.1	13.5	100
0.2	30	0.155	13.12	80
0.3	45	0.321	11.9	21
0.4	60	0.297	10.17	19
0.5	75	0.274	8.44	16
0.6	90	0.250	6.70	16
0.7	105	0.227	4.97	16
0.8	120	0.203	3.24	16
0.9	135	0.180	1.5	16
1.0	150	0.156	-0.23	16

Table 2 The material property parameters of 6061 aluminum

Parameter	$\rho$ ( $\text{kg/m}^3$ )	Young's modulus (E/MPa)	Poisson ration $\mu$	Yield strength $\sigma_s$ (MPa)
value	2750	$6.89 \times 10^4$	0.33	55.2

The vertical section of the computational domain was rectangular with high (h) of 2D and width (w) of 4D, which keep consistent with the experiment. To ensure that the incoming flow was fully developed, also considering the efficiency and accuracy of numerical simulation, the distance from the center of the turbine to the inlet was set as  $L_1$  of 5D, the distance from the center of the turbine to the outlet was  $L_2$  of 20D, total length along flow was L of 25D.

The grids play an important role in numerical simulation and are a representation of geometry. They also have a significant effect on the accuracy and efficiency of the numerical simulation. For the flow field, the hybrid grid, was applied with a structural hexahedral mesh in the flow domain and an unstructured tetrahedral mesh in the rotational domain, was generated by ICEM. After grid independence verification, it could be concluded that nearly seven million elements were reliable with three million elements in the rotational domain, also the minimum average mesh quality was no less than 0.25, The first layer of the grid on blade is 0.0008m.

To give a better evaluation for the pressure pulsation characteristics, the pressure pulsation coefficient ( $C_p$ ) was used to describe the pressure fluctuation, the  $C_p$  was defined as:

$$C_p = \frac{\Delta p}{0.5 \rho U^2} \quad (1)$$

Where  $\Delta p = P_1 - P_{ave}$ , the pressure difference between the at each moment and the mean value,  $\rho =$  density of water ( $\text{kg/m}^3$ ),  $U =$  the velocity of the inlet (m/s).

### Equation discretization and Boundary Conditions

Tidal turbines rotated because of absorbing energy from the tidal current, for solving the problems of rotational motion in the numerical simulation, the sliding mesh was used to simulate rotational motion, the interface was applied to transform the momentum and energy between the rotation domain (turbine domain) and the stationary domain (flow domain). The flow details were simulated by discretizing and solving the energy and momentum equations without considering temperature change, the incompressible Reynolds Averaged Navier-Stokes (RANS) equations are defined as (Sedighi, Akbarzadeh and Salavatipour, 2020)

$$\frac{\partial(\bar{u}_i)}{\partial x_i} + \frac{\partial(\bar{u}_j)}{\partial x_j} + \frac{\partial(\bar{u}_w)}{\partial x_w} = 0 \quad (2)$$

$$\rho \left( \frac{\partial \bar{u}_i}{\partial t} + u_i \frac{\partial \bar{u}_i}{\partial x_i} + u_j \frac{\partial \bar{u}_i}{\partial x_j} + u_w \frac{\partial \bar{u}_i}{\partial x_w} \right) = \rho g - \frac{\partial \bar{p}}{\partial x_i} + \mu \nabla^2 \bar{u}_i + \frac{\partial(-\overline{\rho u_i u_i})}{\partial x_i} + \frac{\partial(-\overline{\rho u_i u_j})}{\partial x_j} + \frac{\partial(-\overline{\rho u_i u_w})}{\partial x_w} \quad (3)$$

Where  $\bar{u}_i$ ,  $\bar{u}_j$  and  $\bar{u}_w$  are the time-average velocity in the  $x$ ,  $y$  and  $z$ ;  $g$  is the gravitational acceleration (m/s);  $\mu$  is the fluid dynamic viscosity.

The term of  $\overline{\rho u_i u_j}$  are called Reynolds stress, the presence of Reynolds stress implies the N-S equations are not closed. So some assumptions are used to close the equations, the Reynolds stress can be expressed as:

$$\tau_{i,j} = -\rho u_i u_j = \mu_t \left( \frac{\partial u_i}{\partial x_j} + \frac{\partial u_j}{\partial x_i} \right) - \frac{2}{3} \rho k \delta_{i,j} \quad (4)$$

Where  $\mu_t$  is turbulent viscosity;  $k$  is kinetic energy and  $\delta_{ij}$  is Kronecker delta.

The SST  $k - \omega$  turbulence model is believed to have a better ability to adapt much severely turbulent flow and has a much higher accuracy and reliability at different types of flows because of combined advantage of  $k - w$  turbulence model and  $k - \epsilon$  turbulence model, the equations are expressed as follow:

$$\frac{\partial(\rho k)}{\partial t} + \frac{\partial(\rho k u_i)}{\partial x_i} + \frac{\partial(\rho k u_j)}{\partial x_j} + \frac{\partial(\rho k u_w)}{\partial x_w} = \frac{\partial}{\partial x_i} \left( \frac{\Gamma_k \partial k}{\partial x_i} \right) + \frac{\partial}{\partial x_j} \left( \frac{\Gamma_k \partial k}{\partial x_j} \right) + \frac{\partial}{\partial x_w} \left( \frac{\Gamma_k \partial k}{\partial x_w} \right) + G \quad (5)$$

$$\frac{\partial(\rho \omega)}{\partial t} + \frac{\partial(\rho \omega u_i)}{\partial x_i} + \frac{\partial(\rho \omega u_j)}{\partial x_j} + \frac{\partial(\rho \omega u_w)}{\partial x_w} = \frac{\partial}{\partial x_i} \left( \frac{\Gamma_\omega \partial \omega}{\partial x_i} \right) + \frac{\partial}{\partial x_j} \left( \frac{\Gamma_\omega \partial \omega}{\partial x_j} \right) + \frac{\partial}{\partial x_w} \left( \frac{\Gamma_\omega \partial \omega}{\partial x_w} \right) + G_w + Y_w + S_w + D_w \quad (6)$$

where  $G$  is the term of generation of dissipation;  $\Gamma$  is the term of effective diffusivity;  $Y$  is the term of dissipation of  $k$ ;  $D$  is the term of cross-diffusion and  $S$  is the eventual user-defined source term.

For those structural problems considering the fluid-solid coupling, fluid is believed to be incompressible inviscid fluid, and solid is considered as elastic solid without considering damping. Those equations included fluid, solid and interface are seen to be governing equation for structural solid, more details can be found in Zhou, Zheng, Kan, Zhang, Wang, Tang and Zhao (2020), the governing equation of structure is shown as follow:

$$M \cdot \ddot{u} + C \cdot \dot{u} + K \cdot u = F \quad (7)$$

Where  $M$  is the mass matrix(kg).  $C$  is damping matrix (N.s/m).  $K$  is the stiffness matrix(N/s).  $u$  is displacement vector of node, m;  $\dot{u}$  is velocity vector, m/s;  $\ddot{u}$  is acceleration vector,  $m^2/s$ .

The Pressure-Based solver was used to solve three-dimensional incompressible flow, the SIMPLE scheme was applied for Pressure-Velocity coupling, a second order for pressure was used, as well as the first-order upwind for turbulent kinetic energy and specific dissipation ration for spatial discretization. The bounded central differencing was used to discrete momentum term in spatial, first-order implicit was adopted for the transient formulation, The time step was set to 360 steps in a revolution for transient simulations at different rotational speeds. To ensure the balance between efficiency and accuracy, the max iteration chosen for each time step was 20 iterations.

For boundary condition, the velocity-inlet boundary condition of 0.4m/s with specified hydraulic diameter and turbulence intensity was adopted at the inlet, pressure-outlet boundary condition with relative pressure of zero was established, free slip wall boundary condition was set for both side walls and no-slip boundary condition was used for runner. Fig. 2 shows the geometric model and grids.

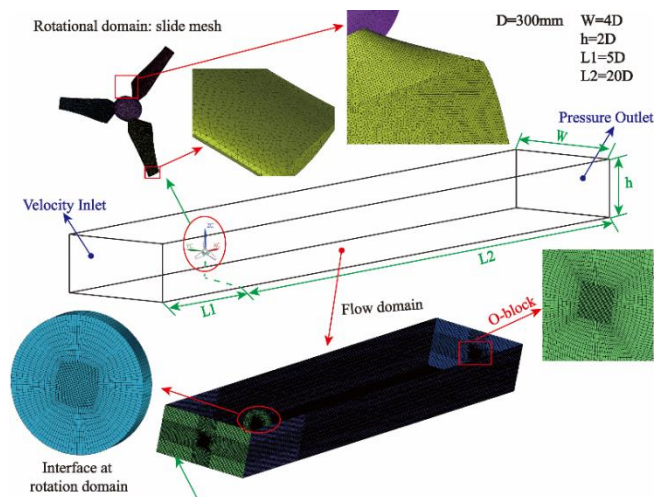


Fig. 2 Geometric model and grids

### Fluid-structure coupling and monitoring points

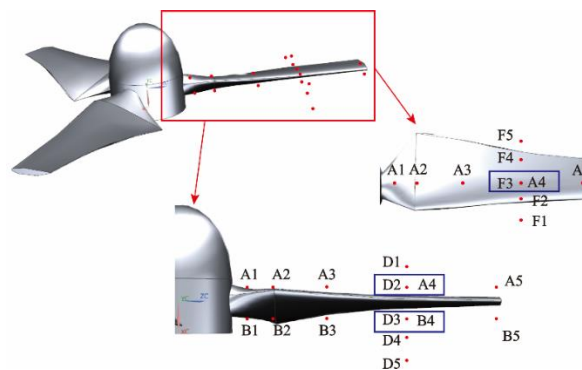


Fig. 3 The distribution of monitoring points

The tidal turbine is working at an environment accompanied with unsteady turbulent flow influenced by the turbine's rotational motion, especially in the swept area where flow velocity gradient changes dramatically around the blades. The blades suffer severely unsteady

pressure pulsation, which may cause negative effects such as flow induced noise, blade deformation, reducing efficiency and so on. To investigate the pressure pulsation characteristics of tidal turbine along the blade vertical axial direction, blade radial and inflow direction, monitoring points were set up at corresponding direction respectively. The distribution of monitoring points is shown in Fig. 3

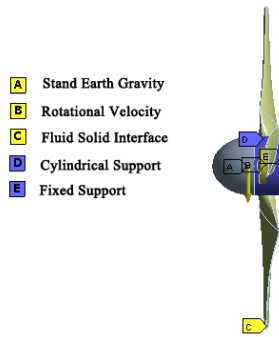
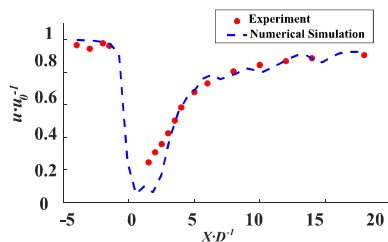
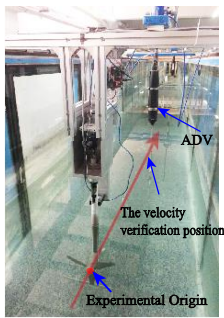


Fig. 4 The diagram of structural constraint

The periodic pressure pulsation generated by the rotational motion will cause fatigue damage to the blades. In addition, the turbine may occur resonance phenomena when the natural vibration frequency of the solid is equal or close to the pressure pulsation frequency, which may cause the obvious blade deformation and even cracked. To quantify the pressure pulsation characteristics and determine the deformation characteristics of the tidal turbine during operation, the bidirectional coupling method was used to solve the structural solid of the tidal turbine. Structural solid was solved by adding constraints combined with results in the fluid fields. In fact, the solving process of structural solid was achieved through force transmission which was established by adding different constraints, the constraints of Fluid Solid Interface was used for transferring hydraulic load of blade surface to structural solid's surface, the hub's axial and radial displacements were fixed and rotating motion was free by adding cylindrical constraints, the gravity was simulated by stand earth gravity and centrifugal force was established due to rotation motion by rotational velocity, the different constraints are shown as Fig. 4.

### Reliability Verification



(a) Model experiment

(b) Velocity comparison between experiments and numerical simulation

Fig. 5 The model experiment and velocity comparison

To validate the accuracy of numerical simulation, the velocity comparisons behind the centre line of the runner between numerical simulation and experiment are presented in Fig. 5, more details about the experiments can be found in (Zhang, Zhang, Lin, Wang, Zhang and Zhao, 2020). The validated case was performed at 10.4 rad/s, it demonstrates velocity between simulations and experiments is quite different in the

range of 0-3D from Fig. 5(b), but the velocity distribution is nearly consistent with experimental velocity. Furthermore, in the far wake, the velocity in the numerical simulation is almost identical to the experimental velocity. The main reasons caused the error are known as follow: there is strong turbulence intensity and anisotropic at near the wake, although turbulence models are predicted and corrected for turbulent flow, relatively large errors are still caused because of assumptions of turbulence models, in addition, the boundary conditions in the numerical simulation may cause some errors compared with actual flow. Above all, it can be concluded that numerical simulation can ensure sufficient accuracy.

For the structural solid of tidal turbine, the unstructured tetrahedral mesh was generated by Ansys Mesh, the grids at blade tip and blade root were refined adopted local size method, blade deformation base on-way FSI(fluid-structure interface) at three different numbers of the grid was used to verify mesh at the 10.4 rad/s, the results are shown as Table 3, it indicates that the blade deformation in case2 and case 3 is nearly similar, so grids at case 2 is believed to be acceptable considering the accuracy and calculation efficiency. The mesh of structural solid is shown in Fig. 6.

Table 3 The comparison of different mesh sizes in structural solid

Case	Global size (mm)	The number of elements	Equivalent stress (Mpa)	Blade deformation ( $\times 10^{-3}$ mm)
1	8	12916	0.38610	9.494
2	4	26466	0.45735	8.835
3	2	115878	0.45857	8.835

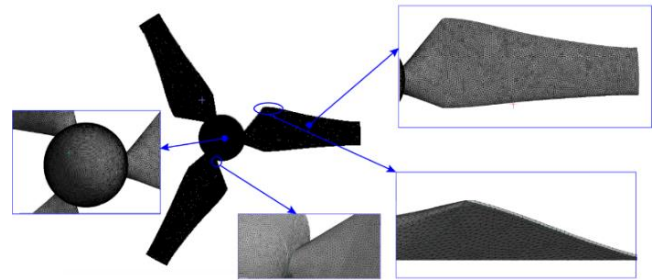


Fig. 6 The mesh of structural solid

## RESULTS AND DISCUSSIONS

### Time domain analysis of pressure pulsation

Fig. 7 shows the pressure pulsation along the radial pressure side at rotational speeds of 9.0 rad/s in the time domain, it can be found that pressure pulsations present a similar tendency at different monitors, but have a different vibration amplitude. In addition, the phase of the pressure pulsation peak gradually lags along the blade radial, the main reason is that blade airfoils lead incoming inflow to flow along blade radial. The amplitude of pressure pulsation gradually increases to a peak at the near middle of blades(A4) followed by decreasing at different rotational speeds. The maximum vibration amplitude of  $C_p$  is near 2.15 located at A4 and the minimum vibration amplitude of  $C_p$  is approximate 0.95 located at A1, the maximum vibration amplitude is about 2.26 times the minimum value. It is worthy to say the pressure pulsations also have a similar tendency at high rotational speed except that the amplitude of pressure pulsation is much stronger, so the curves of  $C_p$  included rotational speeds of 10.4 rad/s and 11.8 rad/s are not shown as follow.

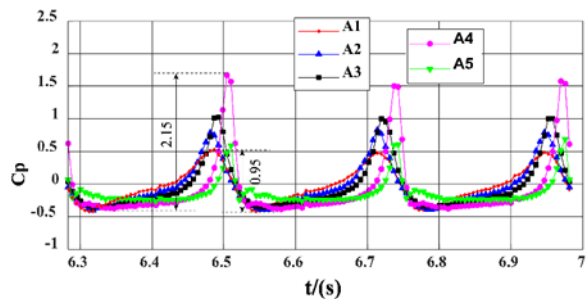


Fig. 7 The Cp along radial pressure side at 9.0 rad/s

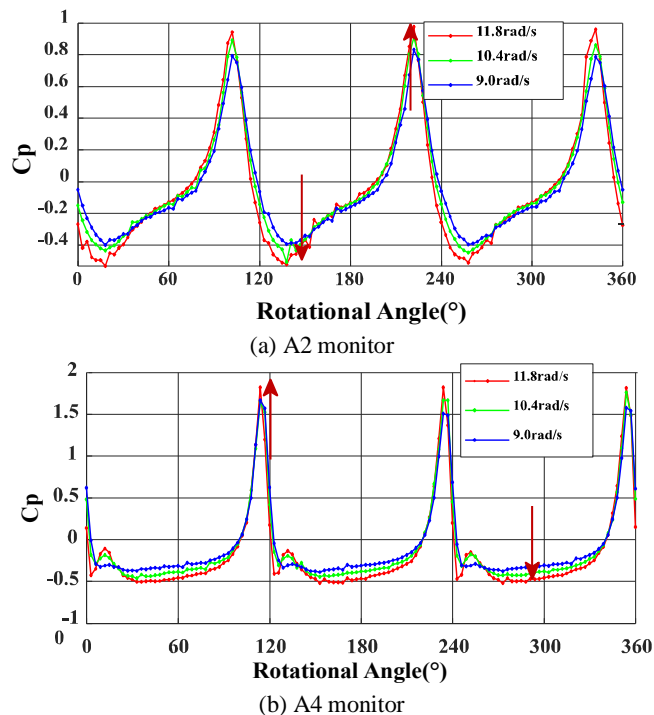


Fig. 8 The pressure pulsation of characteristic monitoring points at different rotating speeds

The simulated Cp at specific monitoring points (A2, A4) in a revolution at different rotational speeds is presented in Fig. 8. It can be found that pressure pulsation along radial pressure side is much stronger as the increase of rotational speeds, the main reason can be concluded that maximum Cp gradually increases and the minimum Cp decreases, it would lead to more unstable instantaneous pressure pulsation on upstream blades.

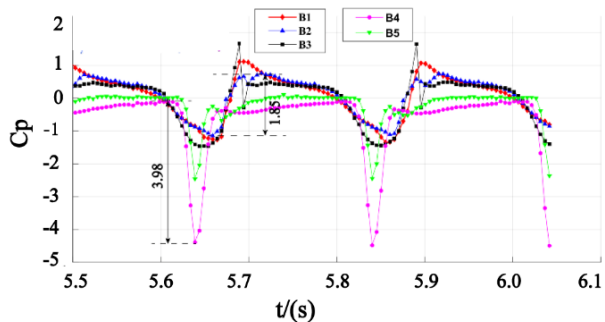


Fig. 9 The pressure pulsation along radial suction side

The simulated Cp along radial suction side at 10.4rad/s is shown in Fig. 9. The lags in the phase of the Cp is different compared with Fig. 7, the phase of minimum Cp is gradually advanced along radial pressure side. At the root of blade suction side, the vibration amplitude at B1 is slightly smaller than at B2 of 1.85, however, the vibration amplitude of 3.98 reaches a peak at B4 followed by a decrease. The pressure pulsations have a similar tendency at high rotational speed, so the curves of Cp include rotational speeds of 10.4 rad/s and 11.8 rad/s are not shown as follow.

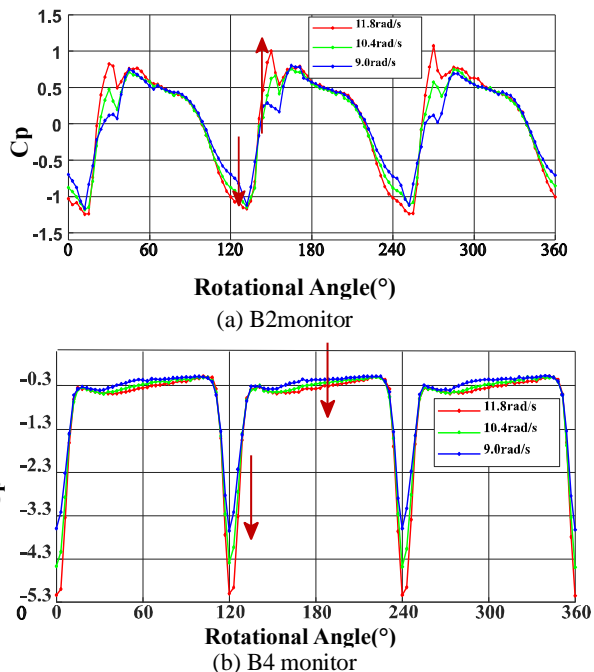


Fig. 10 The pressure pulsation curve at specific points along downstream blade radial

Fig.10 shows the pressure pulsation at specific points (B2 and B4) along radial suction side in a revolution at different rotational speeds. There are some significant differences compared with the amplitude of cp between suction and pressure side. It can be found that maximum Cp at B2 shows an increasing trend as the growth of rotational speeds, the minimum amplitude of Cp shows opposite trend at radial suction side, which is similar with radial pressure side. However, the difference is that both maximum and minimum amplitude of Cp at B4 decrease as the growth of the rotational speeds at radial suction side.

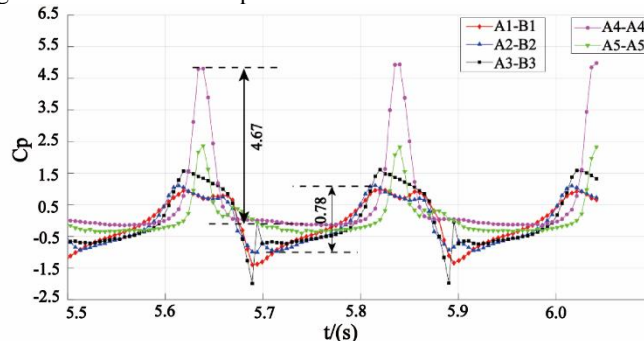


Fig. 11 The difference in pressure pulsation corresponding points both sides of blades

To investigate the variation of pressure pulsation difference on both sides of the blade, the difference of pressure pulsation at 10.4rad/s between

corresponding points at both sides of blades is calculated as Fig. 11. It demonstrates that the characteristic region of pressure pulsation along the blade radial can be mainly divided into three regions, including the region near the blade root, the region from blade root to the middle of the blade, and the region from the middle of the blade to the blade tip. It can be found that the maximum Cp vibration amplitude of 4.67 is located near the middle of the blade (point 4), the minimum value of 0.78 is located at blade root (point 2) along the radial direction, the vibration amplitude shows a slight decrease for point 1 to point 2 with the reason that the hub was designed by a discontinuous airfoil only considering structural strength. The vibration amplitude of Cp trend to increase from blade root (point 2) to the middle of the blade (point 4), the main reason is that lifting force is generated by the three-dimensional airfoils at around this part, at the same time, the fluid gradually generates flow separation near the blade, it all leads a much more serious pressure pulsation, in addition, it also proves that the middle part of the blade is the main part of produce power. The vibration amplitude of Cp tends to decrease from the middle of the blade point 4 to blade tip, it could reduce pressure pulsation amplitude near the blade tip when the fluid in the outer region of the runner is mixed behind the runner.

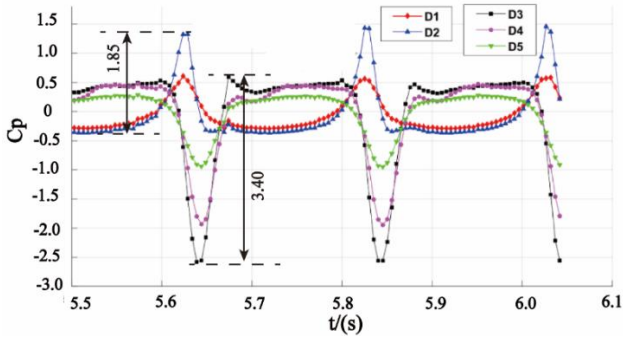


Fig. 12 The pressure pulsation in flow

FIG. 12 shows Cp along the flow direction at 10.4rad/s. It can be found that these points near the blade including D2 and D3 have a larger vibration amplitude of Cp, both Cp and vibration amplitude gradually increase when the inflow flows to the pressure side, however, they present a decreasing trend from suction side to free downstream. Also, the vibration amplitude of approximately 3.40 at the pressure side is larger than 1.85 at the suction side, so it can be said the pressure pulsation is much stronger at the pressure side than it at the suction side.

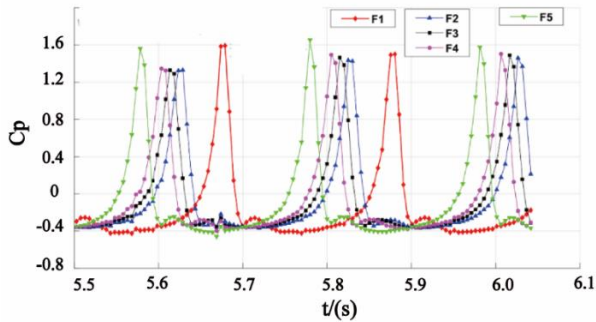


Fig. 13 The Cp along the direction of blade vertical axis

Fig. 13 shows the Cp along the direction of blade vertical axis at 10.4rad/s, it can be found that the Cp amplitude is much stronger at those areas without blade cover including point F1 and F5, it keeps the similar value at the area with blade cover included F2 to F4. The area without blade cover was much easier to exchange energy between kinetic energy and pressure energy to generate much stronger pressure pulsation, the fluid at the area with blade cover is dominated by the blade to generate relatively stable pressure pulsation.

## Frequency domain analysis of pressure pulsation

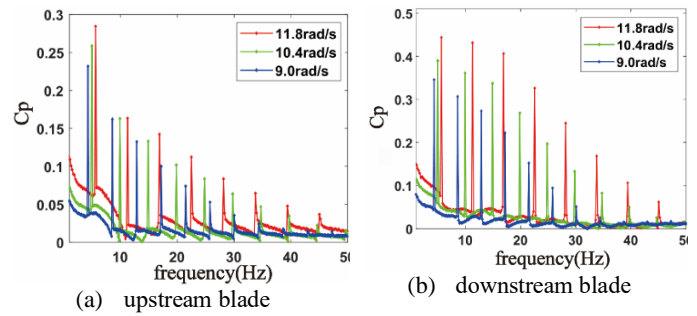
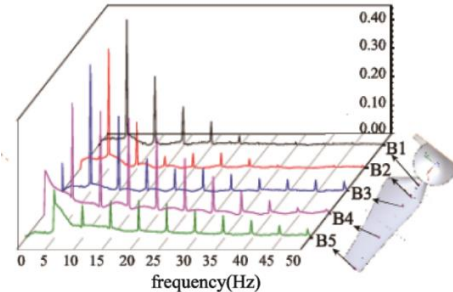
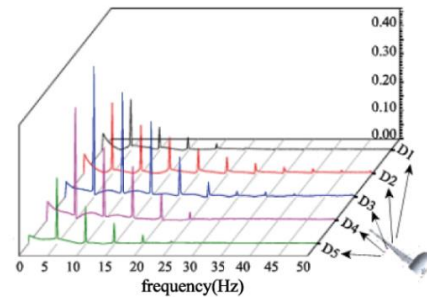


Fig. 14 The frequency at monitor points of A4 and B4 at different rotational speeds along blade radial

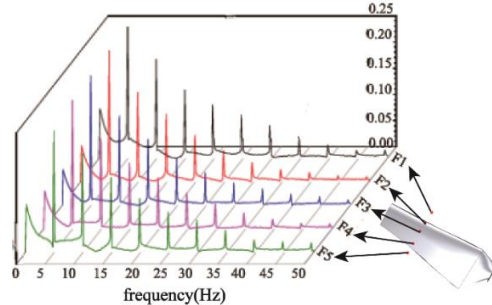
The Fourier transform (FFT) is used to analyze the frequency characteristics of pressure pulsation, Fig. 14 shows the frequency of pressure pulsation located at A4 and B4 along the blade radial at different rotational speeds. It can be found that all of the main frequency of Cp at different rotational speeds is the blade frequency, besides, vibration amplitude increases as the increase of rotational speed. Furthermore, it is obvious that the pressure pulsation at the suction side is much stronger than the upstream blades. The pressure pulsation presents similar frequency distribution at different rotational speeds, so all the next cases are at the 10.4rad/s.



(a) Along downstream blade



(b) Along blade axial



(c) Along blade vertical axial

Fig. 15 The frequency diagram along the blade radial, blade axial, and blade vertical axial

Fig. 15 shows pressure pulsation along the blade radial, blade axial, and blade vertical axial in the frequency domain. The pressure pulsation at blade tip (B5) is smaller than the other location along the radial direction from Fig. 15 (a). Also, abundant frequency doubling is generated from the middle of the blade to the blade tip (B3 to B5). Along the blade axial, blade frequency at the downstream blade (D3) is much stronger, also, the pressure frequency along the axial is mainly dominated by blade passing frequency. Along the direction of blade vertical axial, the main frequency is the same as the other cases, besides, there are much more abundant multi blades-frequency at this case. Above all, we can conclude that the main frequency is the blade frequency at different cases, there are much more abundant multi blade-frequencies along the vertical axial.

### Analysis of bidirectional fluid-solid coupling

Fig. 16 is the average deformation at different rotational speeds. As Fig. 16 shows the average deformation of the blade, is 0.0007mm、0.0011 and 0.0016mm respectively, increases as the increases of rotational speeds. Fig. 17 and Fig. 18 is the average deformation and equivalent stress contour at different rotational speeds. Fig. 17 indicates that the largest deformation occurred near the blade tip, there is little deformation at the blade root as a support structure. In addition, the deformation begins to generate from the middle of the blade and gradually increases to a peak at the blade tip, it is believed that the deformation of the blade is similar to the structure of the cantilever beam, so a maximum deformation generates at the blade tip. The maximum equivalent stress and distribution range increases as the increase of rotational speed as Fig. 18 shows, the equivalent stress distribution of the blade is different from the blade deformation, the maximum equivalent stress is located near the blade root, which is designed as a support structure without considering hydrodynamic design, the stress distribution is spread out along the radial direction as an elliptical shape.

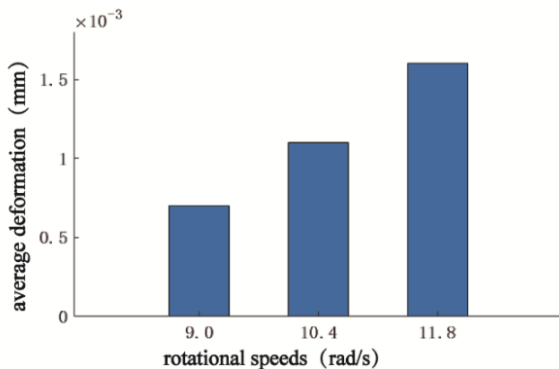


Fig. 16 The average deformation at different rotational speeds

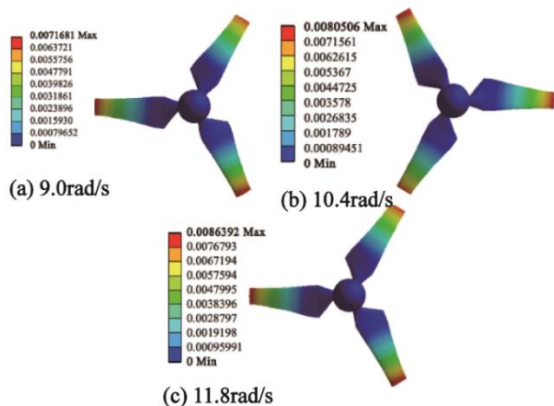


Fig. 17 The average deformation contour at different rotational speeds

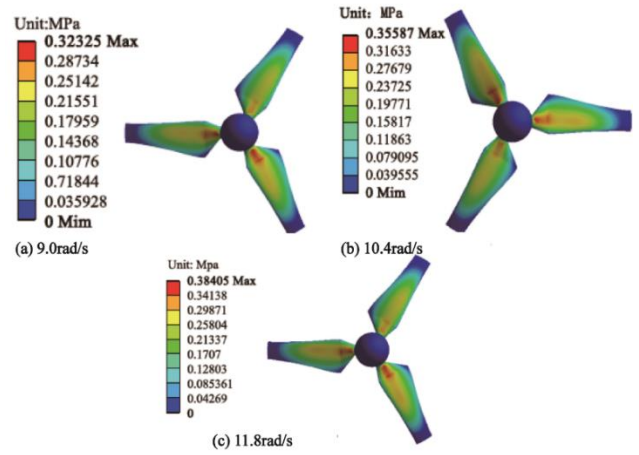


Fig. 18 The equivalent stress contour at different rotational speeds

### Modal analysis

The tidal turbine will produce self-excited vibration for inherent properties such as shape, quality and so on, modal analysis is a numerical method to analyze the self-excited vibration of structural solid. The forms of the modal deformation are generally composed of flapping, sway and coupling of flapping and sway.

Orders	1	2	3	4	5	6
Prestress	57.47	57.66	57.86	139.81	144.71	145.12
No prestress	57.48	57.67	57.89	139.95	144.93	145.98

Table 4 shows the different orders modal frequency at 10.4 rad/s with and without prestress, the modal without prestress refers to the modal affected only by its gravity, in contrast, the modal with prestress refer to the modal affected by the actual force such as gravity, pressure and so on. On the whole, the modal frequency with prestress is slightly higher, but the overall difference is quite small, which indicates that prestress has little influence on the inherent modal of the turbine. In addition, the self-excited frequency is much higher than the main frequency of pressure pulsation, so it is less possible to generate resonance phenomenon.

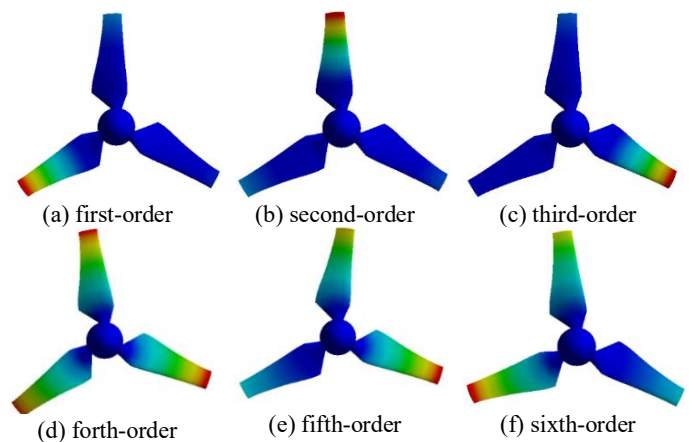


Fig. 19 The different orders' modal deformation with prestress

Fig. 19 shows the first six orders modal deformation contour of the turbine under the condition of prestressed at 10.4 rad/s, it can be found that the first three orders modal deformation mainly is the flapping of a

single blade, the fourth modal is the deformation of a couple of flapping and slight sway, the fifth and sixth modal are deformation a couple of flapping and sway, is accompanied with the deformation generated significant deformation at one blade. Also, the blade may develop certain deflection deformation accompanied with modal deformation. Therefore, for the design of a tidal turbine, both the strength of the blade and the deflection of the material should be considered.

## CONCLUSIONS

Based on Workbench, the system coupling module was used to exchange data, and numerical simulations were simulated based on bidirectional fluid-solid coupling at different rotational speeds. The pressure pulsation coefficient was researched, and the structural deformation and modal characteristics of the tidal turbine were analyzed. The main conclusions are as follows:

(1) The pressure pulsation presents an increase trend as the increase of rotational speed, main frequency is blade frequency at different cases. The pressure pulsation at the suction side is much stronger and has an abundant high-orders frequency. The maximum amplitude of the pressure pulsation along the radial direction is located near the middle of the blade, along the vertical axial direction, the pressure pulsation at the blade covered area is weaker than that in the non-blade covered area.

(2) The increase of rotational speed will lead to the increase of blade deformation and equivalent stress, the maximum deformation is located at the blade tip, blades deformation begins to generate at the middle of the blade. Maximum equivalent stress is located near the blade root, the equivalent stress distribution is spread out along the radial direction as an elliptical shape.

(3) The prestress has little influence on the modal frequency of the tidal turbine. The first to third modal deformation of the tidal turbine is dominated by the flapping with a single blade, the modal deformation from fifth to sixth is a couple of flapping and sway.

## ACKNOWLEDGEMENTS

This work was supported by the National Natural Science Foundation of China (51879159, 52131102), and the National Key Research and Development Program of China (2019YFB1704200), to which the authors are most grateful.

## REFERENCES

- Huang, Y, Wan, DC, and Hu, CH (2021). "Numerical Analysis of Aero-Hydrodynamic Responses of Floating Offshore Wind Turbine Considering Blade Deformation", *The 31st International Ocean and Polar Engineering Conference*, ISOPE, 3, 1880–1888.
- Khalid S, Zhang, L, Zhang, X and Sun, K (2013). "Three-dimensional numerical simulation of a vertical axis tidal turbine using the two-way fluid structure interaction approach", *Journal of Zhejiang University-Science A (Applied Physics & Engineering)*, 14(8), 574-582.
- Park S, Rhee S H (2016). "Influence of blade deformation and yawed inflow on performance of a horizontal axis tidal stream turbine" *Renewable Energy*, 92, 321-332.
- Sedighi H, Akbarzadeh P and Salavatipour A (2020). "Aerodynamic performance enhancement of horizontal axis wind turbines by dimples on blades: Numerical investigation", *Energy*, 195, 117056.
- Tian, WL, Ni, XW, Mao, ZY and Zhang, TQ (2020). "Influence of surface waves on the hydrodynamic performance of a horizontal axis ocean current turbine, *Renewable Energy*, 158, 37-48.

- Ullah H, Hussain M, Abbas N, Ahmad H, Amer M and Noman M (2019). "Numerical investigation of modal and fatigue performance of a horizontal axis tidal current turbine using fluid-structure interaction", *Journal of Ocean Engineering and Science*, 4(4), 328-337.
- Wang, SQ, Sun, K, Xu, G, Liu, YT and Bai, X (2017). "Hydrodynamic analysis of horizontal-axis tidal current turbine with rolling and surging coupled motions", *Renewable Energy*, 102, 87-97.
- Wang, SQ, Cui, J, Ye, RC, Chen, ZF and Zhang, L (2019). "Study of the hydrodynamic performance prediction method for a horizontal-axis tidal current turbine with coupled rotation and surging motion", *Renewable Energy*, 135, 313-325.
- Wang, SQ, Xu, G, Zhu, RQ and Wang, K (2014). "Hydrodynamic analysis of vertical-axis tidal current turbine with surging and yawing coupled motions", *Ocean Engineering*, 155, 42-54.
- Yang, P, Xiang, J, Fang, F and Pain CC (2019). "A fidelity fluid-structure interaction model for vertical axis tidal turbines in turbulence flows", *Applied Energy*, 236, 465-477.
- Zang, W, Zheng, Y, Zhang, Y, Zhang, J and Fernandez-Rodriguez E (2019). "Experiments on the mean and integral characteristics of tidal turbine wake in the linear waves propagating with the current", *Ocean Engineering*, 173, 1-11.
- Zhang, YQ, Zang, W, Zheng, Y, Cappiotti L, Zhang, JS, Zheng, Y and Fernandez-Rodriguez E (2021). "The influence of waves propagating with the current on the wake of a tidal stream turbine", *Applied Energy*, 290, 116729.
- Zhang, YQ, Zhang, JS, Lin, XF, Wang, RS, Zhang, C and Zhao, JL (2020). "Experimental investigation into downstream field of a horizontal axis tidal stream turbine supported by a mono pile", *Applied Ocean Research*, 101, 102257.
- Zhou, Y, Zheng, Y, Kan, K, Zhang, YQ, Wang, HL, Tang, W and Zhao, MS (2020). "Study on hydraulic characteristics of large vertical axial-flow pump used as constant frequency power generation", *Proceedings of the Institution of Mechanical Engineers Part A Journal of Power and Energy*, 235(1)